IOP Publishing Superconductor Science and Technology
Supercond. Sci. Technol. 31 (2018) 055014 (12pp) https://doi.org/10.1088/1361-6668/aab5f9

Test results of a 20 kA high temperature superconductor current lead using *RE*BCO tapes

R Heller, W H Fietz, F Gröner, M Heiduk, M Hollik, C Lange and R Lietzow

Karlsruhe Institute of Technology, Institute for Technical Physics, Karlsruhe, Germany

E-mail: reinhard.heller@kit.edu

Received 11 January 2018, revised 8 March 2018
Accepted for publication 12 March 2018
Published 11 April 2018

Abstract

The Karlsruhe Institute of Technology has developed a 20 kA high temperature superconductor (HTS) current lead (CL) using the second generation material *RE*BCO, as industry worldwide concentrate on the production of this material. The aim was to demonstrate the possibility of replacing the Bi-2223/AgAu tapes by *RE*BCO tapes, while for easy comparison of results, all other components are copies of the 20 kA HTS CL manufactured for the satellite tokamak JT-60SA. After the manufacture of all CL components including the newly developed *RE*BCO module, the assembly of the CL has been executed at KIT and an experiment has been carried out in the CuLTKa test facility where the *RE*BCO CL was installed and connected to a JT-60SA CL via a superconducting bus bar. The experiment covers steady state operation up to 20 kA, pulsed operation, measurement of the heat load at 4.5 K end, loss-of-flow-accident simulations, and quench performance studies. Here the results of these tests are reported and directly compared to those of the JT-60SA CL.

Keywords: current lead, high temperature superconductor, *RE*BCO, fusion magnets

(Some figures may appear in colour only in the online journal)

1. Introduction and objectives

High temperature superconductor (HTS) current leads (CL) in the range of 10–80 kA under fabrication or in operation in accelerator and fusion devices worldwide exclusively use Bi-2223 multi-filamentary material (so-called first generation HTS) embedded in an AgAu matrix [1]. In the frame of the European and German national fusion programme, the Karlsruhe Institute of Technology (KIT) successfully developed the 68 kA HTS CL demonstrator for ITER [2, 3] and developed, constructed and tested the 18.2 kA HTS CLs for the stellarator Wendelstein 7-X [4]. As part of the Broader Approach Agreement between Japan and Europe [5], KIT constructed and tested the HTS CL for the satellite tokamak JT-60SA. In total, six CL for 26 kA for the toroidal field coil system and 20 CL for the central solenoid and poloidal field coils of JT-60SA are needed. Recently KIT has completed this task and details can be found in [6].

Regarding the future use of HTS in CLs, it is indispensable to demonstrate the applicability of the industrially favored *RE*BCO material. Several laboratories are presently investigating the design of a high current HTS connector/CL made with *RE*BCO [7–9]. KIT has developed a 20 kA HTS CL where the HTS part consists of *RE*BCO material. The development consisted of several tasks, i.e. investigations for the selection of stabilizer material [10], optimization and testing of mock-ups for the manufacturing of the 20 kA HTS module using *RE*BCO tapes [11], extended test of the 20 kA *RE*BCO CL, and finally modeling of the *RE*BCO current in steady state and pulsed operation [12]. This paper describes the test results of the CL in steady state and pulsed mode as well as during quench.

To simplify the task and to ease comparison of performance, this CL is identical to that 20 kA JT-60SA CL except the HTS module.

Table 1. Main parameters of the 20 kA *RE*BCO current lead.

Parameter	Unit	Value
Nominal current	kA	20
He inlet temperature for HX, $T_{\mathrm{He,in}}$	K	50
Nominal temperature at warm end of HTS, $T_{100\%\mathrm{HTS}}$	K	60
Length of HX	m	1.206
Outer diameter of HX including cladding tube	m	0.126
Length of HTS module including Cu ends	m	0.480
Outer diameter of HTS module	m	0.118
Number of *RE*BCO tapes/stack		3
Number of stacks in module		24
Contact length between *RE*BCO and Cu end caps	mm	50
Contact resistance at 60 K/4.5 K	nΩ	15/10
Heat load at 4.5 K and $I = 0$ kA	W	~3
Current sharing temperature	K	~80

2. Design of the 20 kA *RE*BCO CL

As already mentioned, the development program consisted of four steps.

1. Selection of superconductor and stabilizer material.
2. Optimization of current transfer from normal conducting parts to *RE*BCO tapes.
3. Construction of a 20 kA CL.
4. Test of the 20 kA CL.

For the selection of the material used for electrical stabilization of the tape in case of a quench, the electrical resistivity and thermal conductivity have to be considered, as electrical stabilization and heat load towards the cold end of the CL have to be carefully balanced. As outcome of material investigations, 12 mm wide brass-stabilized *RE*BCO tapes were chosen for use in the 20 kA *RE*BCO module. Details about the performance and the fabrication of the brass lamination process are given in [10, 11].

In contrast to the multi-filamentary flat Bi-2223 tapes, *RE*BCO tapes are fabricated by depositing the superconducting layer on insulating buffer layers and a highly resistive Hastelloy or nickel–tungsten substrate tape. This allows the current transfer to the superconducting layer only from the side facing the superconducting layer. Therefore, simple stacking of the tapes as performed for the Bi-2223/AgAu tapes is no longer possible. Because of this geometrical structure, the *RE*BCO stacks needed a staircase arrangement at both ends to be able to transfer the current from the copper end caps at the heat exchanger and the cold end part to each *RE*BCO tape individually. A second consequence of the highly resistive barrier caused by the buffer layer and substrate is that a possible current redistribution between the tapes can only be achieved via the ends.

To guarantee thermal stability, a good thermal contact between the tapes, the stabilizer, and the structure is required. Therefore, the soldering between the *RE*BCO tapes, the electrical stabilizer and the structure plays an important role. Mock-ups were fabricated and tested using various solders and soldering techniques. As result of these investigations, a one-step soldering process was chosen to be adequate for achieving a good and reproducible electrical and thermal contact. The selection of In50Sn50 as solder material requires the use of copper cladded *RE*BCO tapes while the copper layer has to be rather thin, i.e., approximately 2 μm, to keep its thermal conductivity within the allowable limit. These tapes were fabricated by SuperOx whereas the brass lamination was performed in house during the manufacturing of the *RE*BCO module. Details can be found in [11].

To allow an easy comparison of the *RE*BCO CL, the layout of the 20 kA JT-60SA CL was used [6], i.e. only the HTS module was changed from Bi-2223 to *RE*BCO.

The design of the 20 kA *RE*BCO CL was adopted from the JT-60SA PF CLs. It consists of

- a resistive copper heat exchanger HX of meander flow type including the room temperature connection. It covers the temperature range from room temperature to 60 K and is actively cooled by 50 K helium gas. The room temperature connection is realized by conventional water-cooled copper cables.
- an HTS module covering the temperature range from 60 to 4.5 K cooled by heat conduction from the low temperature end. Here, 72 *RE*BCO HTS tapes were used which are grouped in 24 three-fold stacks with staggered ends to provide low-resistive contacts to the copper end caps for each tape.
- a low temperature connection to the superconducting feeder at 4.5 K equipped with a Nb_3Sn insert to reduce the resistive losses. This technique was developed in the past for the conventional CL built for various magnet projects at KIT [13, 14].

Table 1 summarizes the main parameters of the *RE*BCO CL whereas in table 2 the parameters of the *RE*BCO and Bi-2223 modules are given. The material property data are taken from [10].

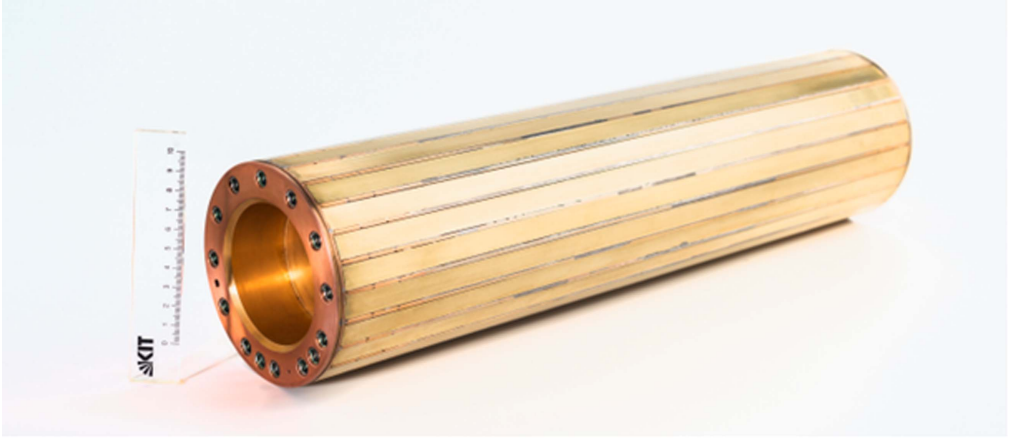

Figure 1. Picture of the completed 20 kA *RE*BCO module.

As all parts of the manufacturing and assembly of the 20 kA *RE*BCO CL except the HTS module are identical to those of the JT-60SA CLs, we refer to [5] for details. The assembly of the *RE*BCO module is described in [11]. Figure 1 shows a picture of the *RE*BCO module after completion.

The *RE*BCO CL was instrumented with temperature sensors and voltage taps identical to those of the JT-60SA CLs: three temperature sensors (TVO sensors at the cold and warm end of the HTS module and a Pt100 sensor at the room temperature end of the CL) are used for operation control. Various voltage taps were used to measure the voltage along the HTS module in case of a quench and along the heat exchanger. All sensors were duplicated for redundancy reasons. Two heater cartridges of 500 W each are installed in the RT terminal, which are controlled by the Pt100 sensor to avoid freezing of the water cooling the copper cables. Additionally, eight temperature sensors (Pt1000) and 16 voltage taps are attached to the *RE*BCO module to measure

- the temperature profile along the *RE*BCO module ($T\_30\%$, $T\_50\%$, $T\_70\%$, $T\_90\%$),
- the temperature on four selected *RE*BCO stacks close to the warm end copper contact where the maximum temperature during quench should occur ($T\_01\_95\%$, $T\_07\_95\%$, $T\_13\_95\%$, $T\_19\_95\%$),
- the voltage along the cold and warm end on the same four *RE*BCO stacks (V_01, V_07, V_13, V_19 at cold and warm end each).

Figure 2 displays the temperature sensors T and voltage sensors V, together with the quench detector (QD) and the heater. Figure 2(a) shows the sensors of the CL, figure 2(b) shows the additional temperature and voltage sensors along the *RE*BCO module, and figure 2(c) shows the additional temperature sensors at 95% and voltage sensors around the *RE*BCO module.

After final assembly of the *RE*BCO CL, it was installed in the CuLTKa test facility at KIT [15] to test it together with a 20 kA JT-60SA CL. Both CLs were connected via a superconducting bus bar made of NbTi that had already been used during the acceptance tests of the JT-60SA CLs.

Table 2. Main parameters of the 20 kA *RE*BCO module and comparison to the Bi-2223 module.

Parameter	Unit	*RE*BCO	Bi-2223
Tape width	mm	12	4
Number of tapes		72	360
Critical current of tape at 77 K, s.f.	A	368	110
Superconductor area	mm^2	1.296	126.72
Total tape area incl. stabilizer and solder	mm^2	397.44	370.01
Stainless steel area	mm^2	1320	1308
Electrical stabilizer area: Brass (*RE*BCO) or AgAu (Bi-2223)	mm^2	259.2	190.08
Effective length of HTS stacks	m	0.350	0.390
Stabilizer resistivity at 90 K	nΩm	40.0	14.40
R/L of stacks	$\mu\Omega\ mm^{-1}$	0.154	0.076

3. Results of *RE*BCO CL testing

After cool-down of the test arrangement within four days and thermal stabilization during the following weekend, the experiment was carried out according to the test program.

1. Heat load measurements at 4.5 K without current for different temperature differences along the HTS module to separate the heat load from the CL from the background losses.
2. Steady state operation at 10, 14, 16, 18, and 20 kA.
3. Pulse tests with trapezoidal current pulses of ramp rates of 1 and 10 kA s^{-1}.
4. Loss-of-flow-accident (LOFA) tests at 16, 18, and 20 kA.
5. Enhanced quench tests at 20 kA.

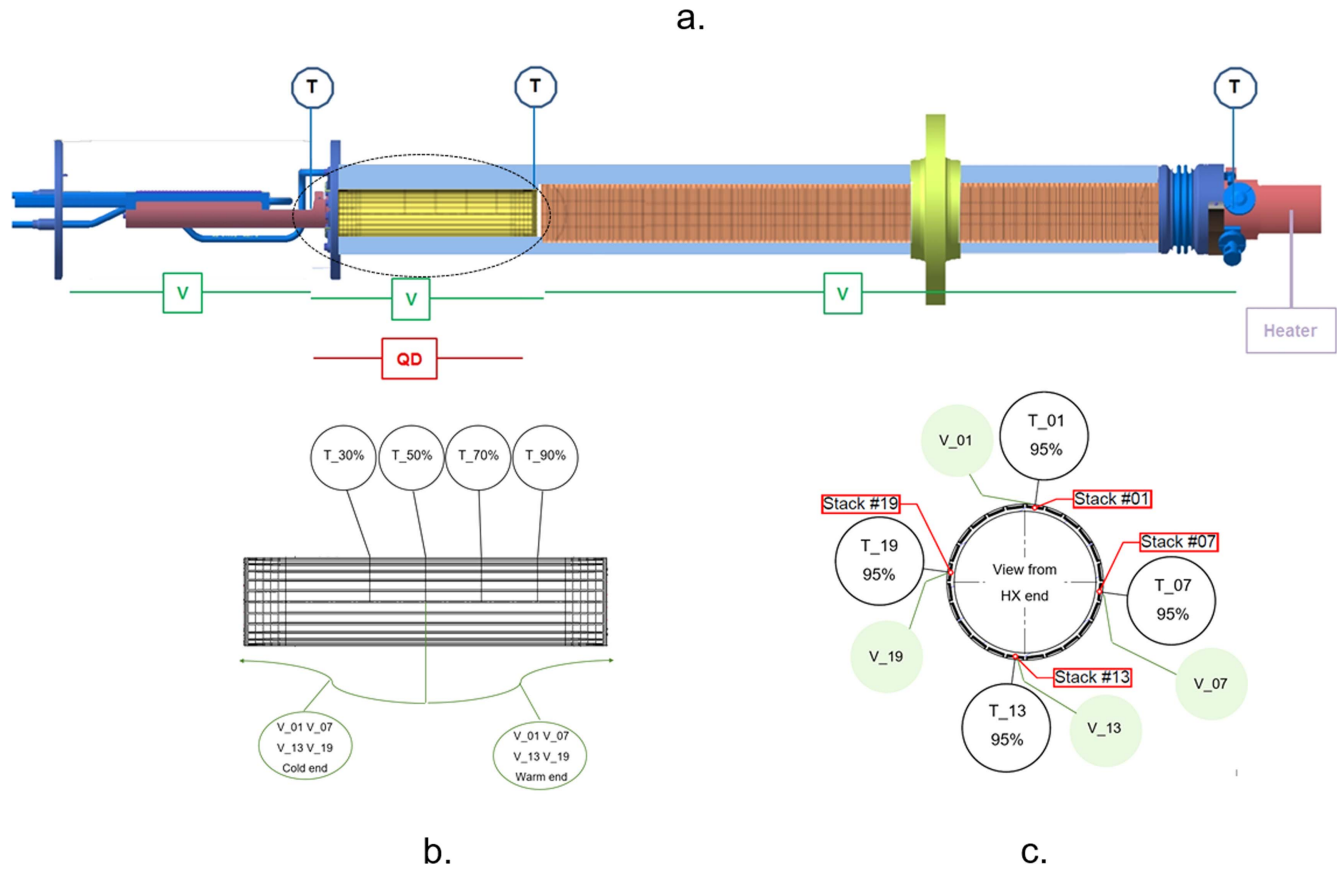

Figure 2. Temperature sensors *T* and voltage sensors *V*, together with the quench detector (QD) and the heater: (a) sensors of the current lead, (b) additional temperature and voltage sensors along the *RE*BCO module, (c) additional temperature sensors at 95% in length counted from cold end and voltage sensors around the *RE*BCO module.

In the following, the results of the different tests are presented and compared to those of the JT-60SA CL where Bi-2223 material is applied.

3.1. Heat load measurements at 4.5 K without current for different temperature differences along the HTS module

The aim of this measurement series was to separate the background losses of the test cryostat from the heat load of the CLs. Figure 3 shows the measured heat load at 4.5 K as a function of the temperature difference along the HTS module for the *RE*BCO and for comparison that for the Bi-2223 CL. Both CLs show very similar heat loads for the experiments performed with a $T_{\mathrm{He,in}} = 20$ K, 50 K, and 70 K which results in temperatures at the warm end of the HTS module of 30 K, 60 K, and 80 K leading to a temperature difference from the cold end at 4.5 K to the warm end of the HTS module of approx. 25 K, 55 K and 75 K, respectively. The results of design calculations for the *RE*BCO CL are also given as lines. Here the dashed line represents the calculation results that consider only the CL [11]. In addition, the result of calculations which includes the contribution of the vacuum shell is shown as solid line. There is a good agreement between experimental data and calculation. Details on the contributions of the additional heat load caused by thermal conduction of the vacuum shell of the CL to the heat load at 4.5 K can be found in [16].

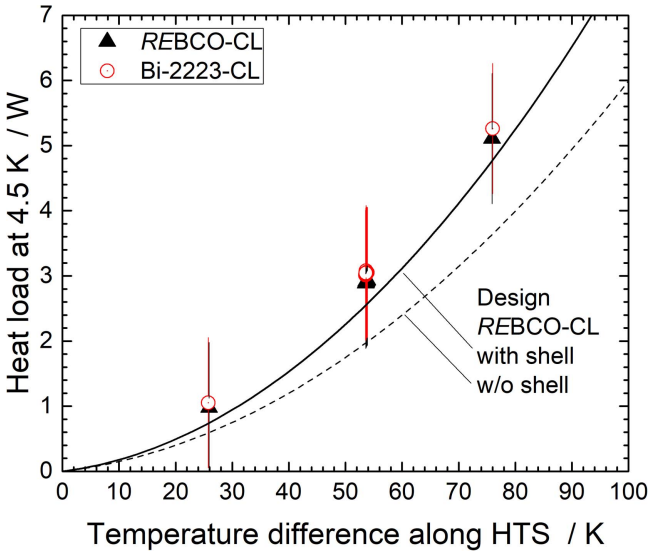

Figure 3. Measured heat load as a function of the temperature difference along the HTS module for the *RE*BCO and for comparison for the Bi-2223 current lead. The results of design calculation for the *RE*BCO current lead without (dashed line) and with (solid line) the contribution of the vacuum shell are shown as well.

3.2. Steady state operation at 10, 14, 16, 18, and 20 kA

The steady state current operation was executed for 10, 14, 16, 18 and finally 20 kA with a stepwise increase. For these

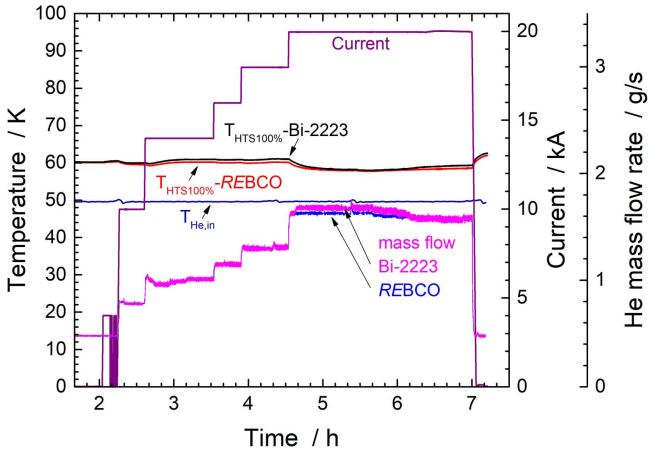

Figure 4. He temperature at the inlet of the heat exchangers, $T_{\text{He-in}}$, the temperatures at warm end of the HTS module, $T_{\text{HTS100\%}}$, the operation current and the He mass flow rates through the HX.

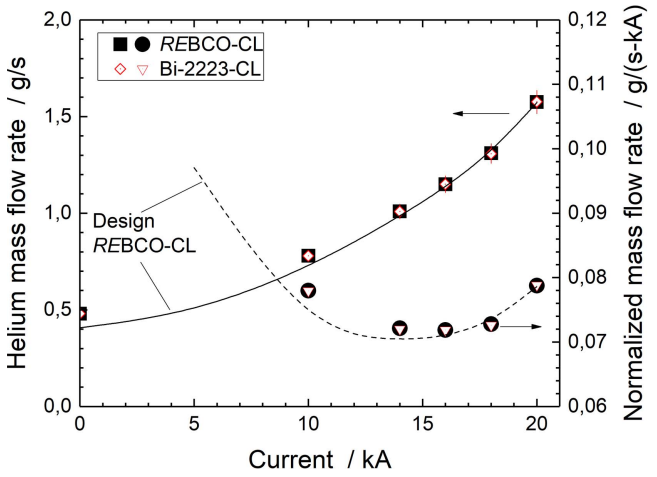

Figure 5. Measured He mass flow rate $\dot{m}$ through the HX and specific He mass flow rate $\frac{\dot{m}}{I}$ for the *RE*BCO (full symbols) and Bi-2223 (open symbols) current leads as a function of the operation current. The error bars indicate the measurement error of the flow meter. The results of the design calculations (solid and dashed line) are also shown.

tests, the QD level for the HTS module was set to 10 mV and the QD delay time to 100 ms. A current ramp-up speed of 100 A s^{-1} was chosen. The helium mass flow was increased at nominal inlet temperature of 50 K in accordance to the operation current to accommodate higher resistive dissipation at higher current levels. Figure 4 shows the He temperature at the inlet of the heat exchangers, $T_{\text{He-in,HX}}$, the temperatures at warm end of the HTS module, $T_{\text{HTS100\%}}$, the operation current and the He mass flow rates through the heat exchanger. For 20 kA, $T_{\text{HTS100\%}}$ is lower than 60 K which is caused by the fact that the CL is optimized for a steady state current of 16 kA. This can also be seen from figure 5, which shows the measured He mass flow rate $\dot{m}$ through the heat exchanger and the specific He mass flow rate $\frac{\dot{m}}{I}$ which is the mass flow rate normalized to the related current for the *RE*BCO (solid symbols) and Bi-2223 leads (open symbols) as a function of the operation current. The error bars indicate the measurement error of the flow meter. The result of the design calculations (solid and dashed line) is also shown. Both CLs behave very similar.

Special attention has been given to the contact resistances between the *RE*BCO module and the cold end R_C and between the *RE*BCO module and the heat exchanger R_W. For the evaluation of R_C and R_W, different voltage taps and methods are available.

- Electrical method: determination of
  - clamp contact resistance between the CL and the 4.5 K bus bar: R_{clamp},
  - sum of contact resistances: $R_{\text{HTS}} = R_C + R_W$.
- Calorimetric method: resistance calculated from the heat load at 4.5 K with current: $R_{\text{calo}} = R_{\text{clamp}} + R_C$. R_{calo} has been obtained by taking the slope of the heat load data at 4.5 K as a function of the square of the current.

Taking these three quantities, it is possible to evaluate R_C and R_W:

$$R_C = R_{\text{calo}} - R_{\text{clamp}}$$
$$R_W = R_{\text{HTS}} - R_C. \quad (1)$$

Furthermore, the voltage measured at the cold and warm end of four stacks are taken and linked to the average stack current $I_{\text{stack}} = I_{\text{op}}/24$. Of course, this is a rough estimate but the best one available. From the resultant resistances $R_{\text{stack},C}$ and $R_{\text{stack},W}$, and assuming that these resistances are representative for all 24 ones, equivalent R_C and R_W are calculated. Table 3 summarizes the results—for comparison the numbers of the Bi-2223 CL are presented, too. It can be concluded that the contact resistances of the *RE*BCO module are larger than those of the Bi-2223 module; further, the ratio R_W/R_C is 1.72 for *RE*BCO and 2.08 for Bi-2223. The contact resistances $R_{\text{stack},C}$ and $R_{\text{stack},W}$ extrapolated from contact voltages of four specific stacks differ by about 10% from those calculated from R_{clamp}, R_{HTS}, and R_{calo}. This result suggests that the current distribution should not be very inhomogeneous. Comparing the experimental results to those obtained with a 2D electric model [11], there is an underestimation of the calculations by ~20%. This supports the conclusion that the 24 three-fold stacks of the *RE*BCO module behave very similar to the three-fold stack mock-up investigated in [11], which demonstrates that the soldering process is reliable.

Figure 6 shows the measured temperature profiles along the *RE*BCO module (symbols) for various currents and different He inlet temperatures $T_{\text{He,in}}$ and the comparison to the design calculations (lines) [11]. The calculated temperatures along the *RE*BCO module coincide nicely with the measured ones for temperatures above 50 K while they deviate below. This is caused by the fact that the temperature dependence of the resistance of the Pt1000 sensors gets worse at temperatures below 50 K approaching a lower limit at about 20 K. So the data of temperature sensor *T*_30% is not shown in figure 6.

3.3. Pulse tests with trapezoidal current pulses for ramp rates of 1 and 10 kA s^{-1}

The scope of these tests was to demonstrate the performance of the HTS CL in pulsed operation at the rated current of

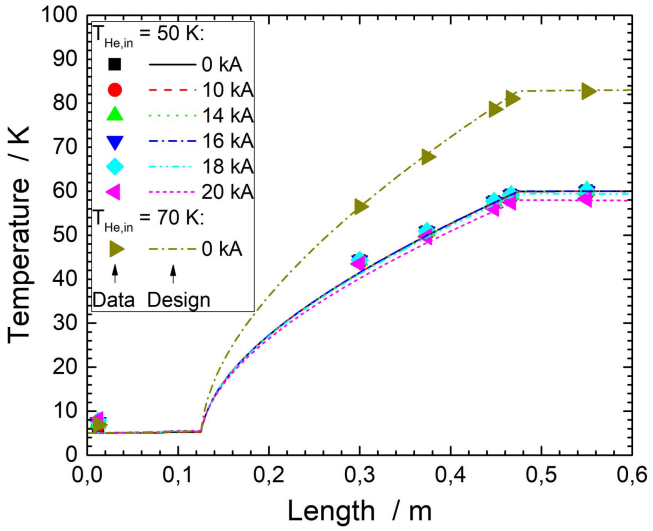

Figure 6. Measured temperature profiles along the *RE*BCO module (symbols) for various currents and comparison to the design calculations (lines).

20 kA for fast ramp rates of 1 and 10 kA s^{-1}. One hundred trapezoidal pulses with equal flat top and idle times of nominal 30 s, each, were performed which is long enough to obtain stable conditions for the CL. For these pulse scenarios, it is important to know the average He mass flow rate required during the pulsed operation. For this an averaged steady state current I_{av} was computed according to the following equation (which is based on equalizing the average energy for both current cases):

$$\frac{E}{R} = I_{av}^2 T = \int_0^T I(t)^2 \mathrm{d}t, \tag{2}$$

where T is the total pulse time, i.e. 100 s per pulse for a ramp rate of 1 kA s^{-1} and 64 s for 10 kA s^{-1}. The resultant current is $I_{av} = 14.14$ kA—i.e. independent of the ramp rate—and the corresponding design He mass flow rate is 0.99 g s^{-1}.

In the experiment, the ramp up and down and the time at full current could be adjusted correctly. However, due to the necessary manual adjustment of the pulse repetition time, the idle times were not equal to the nominal 30 s, but 34 s for the 1 kA s^{-1} pulses and 31 s for the 10 kA s^{-1} pulses. Therefore, the average currents I_{av} and consequently the optimal He mass flows rates differ from the nominal ones.

Figure 7 shows the temperature at the warm end of the *RE*BCO- and Bi-2223-modules $T_{HTS100\%}$ and the current for the trapezoidal pulsing with ramp rates of 1 kA s^{-1} (left) and 10 kA s^{-1} (right). Exponential fits to the data are also shown. The resultant behavior of the CLs is different for the 1 kA s^{-1} and 10 kA s^{-1} pulses because for both ramp rates, the same helium mass flow rate of 0.99 g s^{-1} was used.

The results of the pulse tests are summarized as follows.

- At the beginning of the pulsing, the temperature $T_{HTS100\%}$ reduces because the helium mass flow rate is increased. The $T_{HTS100\%}$ decrease is larger for the 1 kA s^{-1} than for the 10 kA s^{-1} ramp rate because of the significantly different average current (12.9 kA for 1 kA s^{-1} and 13.855 kA for 10 kA s^{-1}). After some time the temperature increases again reaching a stable condition after about 1 h for the 1 kA s^{-1} ramp rate whereas for the 10 kA s^{-1} ramp rate no fully stable condition was reached even after 2 h when the pulsing was stopped. From the exponential fit it is concluded that after 3 h operation this should be achieved. The temperature increase is significantly larger for the 10 kA s^{-1} pulses caused by the higher average current due to the shorter idle time of 31 s. The total temperature increase during pulsing is 0.25 K and 1.5 K for 1 kA s^{-1} and 10 kA s^{-1} ramp rates, respectively. Checking the temperature variation during one of the multiple current pulses in figure 7, a marginal temperature increase of $T_{HTS100\%}$ of about 0.2–0.3 K is observed.
- During one pulse cycle, the temperature at RT-end changes by less than 1 K. A larger change is observed during the whole pulse scenario that is influenced by the heater operation controlled by T_{RT} switching on for $T_{RT} < 290$ K and switching off for $T_{RT} > 290$ K with a time constant of about 10–15 min.

During the pulse tests, the losses at the cold end consist of the conductive losses by heat conduction through the CL, resistive losses in the cold end copper part and the clamp contact, and AC losses during the current ramping.

$$P_{total} = P_{cond} + P_{joule} + P_{AC}, \tag{3}$$

where P_{cond} = heat load from heat conduction through the CL, P_{joule} = resistive losses at the cold end of the CL, and P_{AC} = AC losses during pulsing. The AC losses consist of different parts

$$\begin{aligned} P_{AC} &= P_{BB} + P_{Cu\text{-}bar} + P_{HTS} \\ P_{BB} &= P_{coupl\text{-}NbTi} + P_{hyst\text{-}NbTi} + P_{JB} \\ P_{Cu\text{-}bar} &= P_{ec} + P_{coupl\text{-}Nb3Sn} + P_{hyst\text{-}Nb3Sn} \\ P_{HTS} &= P_{coupl\text{-}stack} + P_{hyst\text{-}stack}, \end{aligned} \tag{4}$$

where P_{BB}, $P_{Cu\text{-}bar}$, and P_{HTS} are losses in the NbTi bus bar, the cold end copper bar and the HTS stacks. The losses in the NbTi bus bar consist of the coupling and hysteretic losses, $P_{coupl\text{-}NbTi} + P_{hyst\text{-}NbTi}$, and of the eddy current losses in the joint box P_{JB}. The losses in the cold end copper bar consist of the eddy current losses in the copper bar P_{ec} and of the coupling and hysteretic losses in the Nb_3Sn insert, $P_{coupl\text{-}Nb3Sn} + P_{hyst\text{-}Nb3Sn}$. The losses in the HTS stacks consist of the coupling and hysteretic losses, $P_{coupl\text{-}stack} + P_{hyst\text{-}stack}$.

The AC losses were measured calorimetrically by considering the enthalpy change in the helium flowing in the part of the bus bar circuit connected to the *RE*BCO- and Bi-2223 CL. From these values, the ohmic contribution due to the current flowing in the resistive parts of the cold end and the conductive heat load from the CL were subtracted. They were measured to be negligible for the 1 kA s^{-1} ramp rate and about 0.2 W for 10 kA s^{-1} ramp rate but with a large error bar. During the pulse tests of the W7-X Bi-2223 CLs, the different loss contributions were evaluated [17]. A similar calculation taking into account the actual dimensions of the

Table 3. Summary of measured and evaluated resistances at cold and warm contacts of the *RE*BCO module and comparison to Bi-2223.

Parameter	*RE*BCO module	*RE*BCO module (from three-fold stack resistance)	2D model [9]	Bi-2223 module
R_{clamp} (nΩ)	(2.36 ± 0.03)	—	—	(2.54 ± 0.02)
R_{HTS} (nΩ)	(27.71 ± 0.06)	—	22.71	(18.89 ± 0.18)
R_{calo} (nΩ)	(12.54 ± 0.43)	—	—	(8.67 ± 0.39)
R_C (nΩ)	(10.18 ± 0.43)	(11.04 ± 1.29)	8.66	(6.13 ± 0.39)
R_W (nΩ)	(17.53 ± 0.44)	(15.13 ± 1.29)	14.05	(12.76 ± 0.43)

*RE*BCO and Bi-2223 CLs and of the bus bar together with the coupling time constant of the NbTi bus bar as given in [18] led to numbers, which are in fair agreement to the data.

Table 4 summarizes the main results of the pulse tests.

It is possible to operate the *RE*BCO CL with a constant mass flow rate safely, i.e., no flow regulation is necessary. This result was already achieved for the JT-60SA CL tests [6].

3.4. LOFA tests at 16, 18, and 20 kA

Loss of helium mass flow simulations were performed for the *RE*BCO CL at 16, 18, and 20 kA. The quench detection voltage threshold was set to $V_{QD} = 10$ mV. From these tests, the time from stoppage of the mass flow rate until a quench occurs and the 'current sharing temperature' was evaluated. For clarification, it has to be noted that it is not possible to define a current sharing temperature for a specific electric field of e.g. 1 μV cm^{-1} as it is commonly used in characterization of single tapes. Due to the temperature gradient along the HTS module, the critical current (and current sharing temperature) is not constant and so it is not possible to define a normal length for a specific voltage. Therefore, a voltage criterion was chosen to determine the current sharing temperature and the following correlation (analog to the one for the critical current) has been used:

$$V(T) = V_C \left(\frac{T}{T_{CS}}\right)^n. \quad (5)$$

Here V is the voltage, T the temperature, V_C is the voltage criterion, T_{CS} the current sharing temperature, and n is the index term.

The measured voltage drop along the HTS module includes both copper end caps which results in a resistive contribution, which increases quasi-linearly with temperature. At a specific temperature, the voltage drop starts increasing more than linearly. This leads to the following correlation:

$$V(T) = V_0 + \frac{dV}{dT}T + V_C\left(\frac{T}{T_{CS}}\right)^n. \quad (6)$$

T_{CS} was defined for a voltage drop of 10 μV, which is significantly beyond the voltage resolution of approx. 2 μV. In addition, a quench temperature T_Q was defined for a voltage drop of 0.5 mV. Equation (6) was fitted to the $V(T)$-data to get T_{CS} and T_Q. Comparing data and fit, a systematic shift of the fitted T_{CS} to higher values was observed while there is no shift of T_Q. This shift can be explained by the presence of current redistribution between the stacks leading to an additional voltage. An additional uncertainty is present due to the voltage resolution that results in a larger error of T_{CS} than of T_Q.

Figure 8 shows the temperature $T_{HTS100\%}$ and voltage along the HTS module after subtraction of the linear part of equation (6) as a function of time during LOFA at 20 kA for the *RE*BCO and Bi-2223 CLs. A direct comparison to the results of single stack measurements presented in [11] is not possible because for the single stack the voltage has been measured at liquid N_2 as a function of the transport current while here the voltage was measured during temperature increase for constant current.

Figure 9 shows the voltage along the HTS module as a function of the temperature $T_{HTS100\%}$ for 16, 18, and 20 kA. For comparison, the typical result of a Bi-2223 CL (JT-60SA) is also shown.

The current sharing temperature T_{CS} (defined as discussed before) at 20 kA is at 79.2 K for the *RE*BCO CL and 84.6 K for the Bi-2223 CL. The quench temperature T_Q (defined as discussed before) is 81.3 K for the *RE*BCO CL and 91.0 K for the Bi-2223 CL. The current sharing is much broader in case of Bi-2223 than for *RE*BCO; one reason is the much higher critical temperature of Bi-2223 compared to *RE*BCO. In addition, the lower electrical resistance of the AgAu matrix (Bi-2223) compared to brass (*RE*BCO)—see table 2—helps in increasing the temperature margin. Consequently, the time from stoppage of the helium mass flow rate until the quench occurs, is significantly smaller for *RE*BCO but still large enough to allow reaction of the operator.

Table 5 summarizes the main results of the LOFA tests. Here the LOFA time is defined as the time starting from switch-off of the helium mass flow rate until reaching 10 mV.

The contact voltage of the four stacks at the warm and cold end was used to study possible current redistribution during current sharing. Figure 10 shows the voltage of the four stacks at the warm and cold end during LOFA at 20 kA. The voltages of stacks #13 and #19 develop earlier than of #1 and #7. The current redistribution can be seen more clearly if looking to the voltage at the cold end as this can only happen via the contacts. It looks like stack #1 and #7 carry less current than #13 and #19. Of course, this is a qualitative result as only four out of 24 stacks are equipped with voltage taps and the current flowing in each stack is not known.

The current sharing temperatures measured during the LOFA simulation tests were compared to the expected

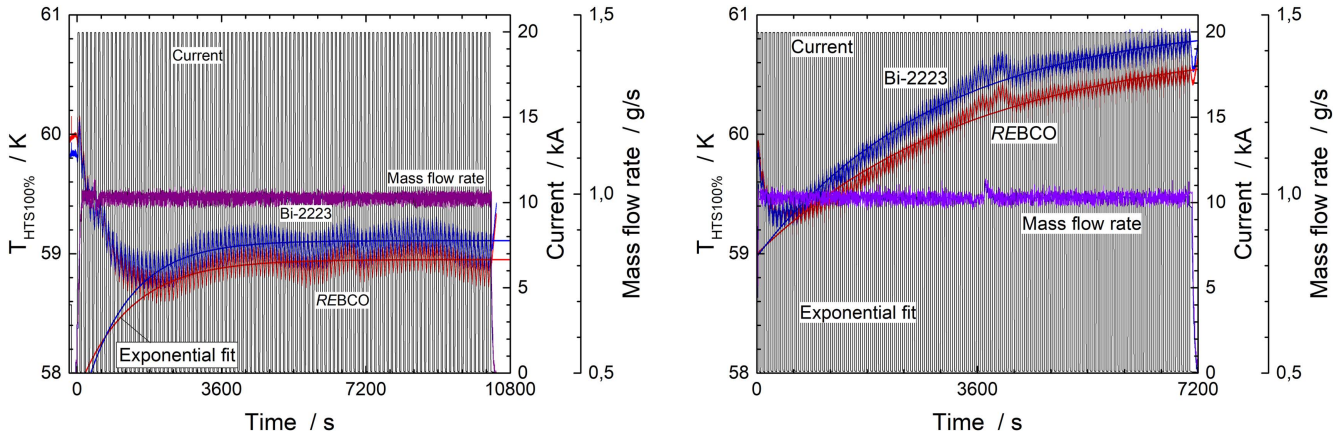

Figure 7. Temperature at the warm end of the *RE*BCO- and Bi-2223-modules $T_{HTS100\%}$ and the current for the trapezoidal pulsing with ramp rates of 1 kA s^{-1} (left) and 10 kA s^{-1} (right). Exponential fits to the data are also shown.

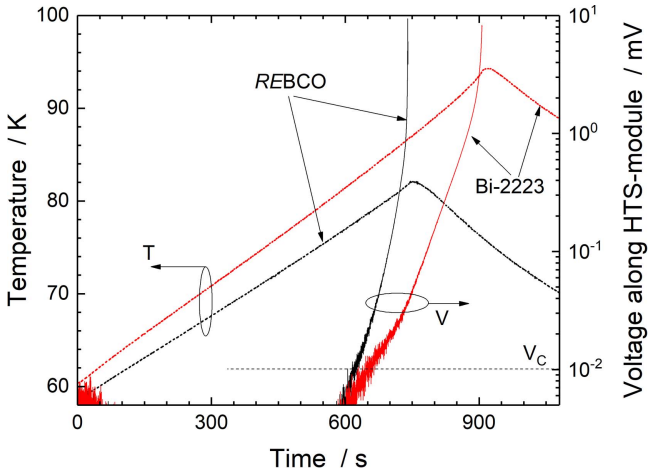

Figure 8. Temperature $T_{HTS100\%}$ and voltage along the HTS module after subtraction of the linear part as a function of time during LOFA at 20 kA for the *RE*BCO and Bi-2223 current leads. The voltage criterion $V_C = 10\ \mu$V is also shown as a dashed line.

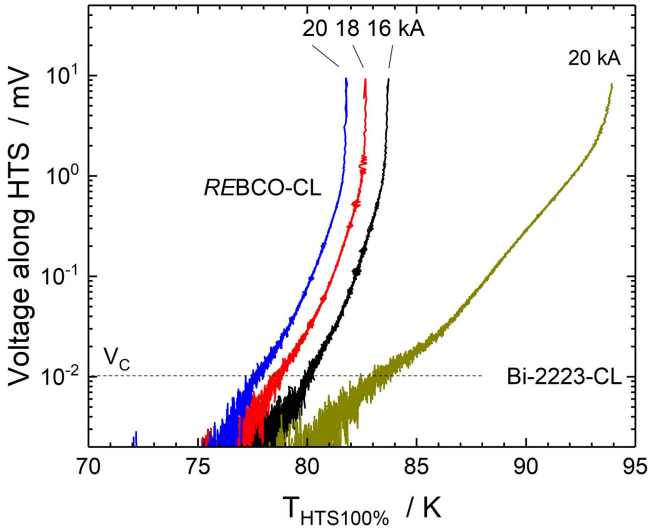

Figure 9. Voltage along the HTS module as a function of the temperature $T_{HTS100\%}$ for 16, 18, and 20 kA. For comparison, the typical result of a Bi-2223 current lead (JT-60SA) is also shown. The voltage criterion $V_C = 10\ \mu$V is shown as a dashed line.

numbers scaled from single tape measurements [11]. Figure 11 shows the critical current expected from single tape data taking into account the load line of the *RE*BCO module at average and maximum magnetic field perpendicular ($B_{\perp,av}$ and $B_{\perp,max}$) and parallel ($B_{||,av}$ and $B_{||,max}$) to the *ab*-plane as a function of temperature and the measured current sharing temperature T_{CS} and quench temperature T_Q. The data which correspond to 10 μV are close to the $I_c(T)$ line for $B_{\perp,max}$ whereas T_Q is above the line for $B_{\perp,av}$. The conclusion is that current sharing started below the expectation but this is influenced by the current distribution between the tapes within the individual stack [11] and between the stacks as well. Taking this into account, the experimental results are within the expectations.

3.5. Enhanced quench tests at 20 kA

At 20 kA, several LOFA tests were performed with different quench detection level V_{QD} to study the quench behavior. This was the only way to study the quench behavior but should be similar to a quench initiated by other sources because the HTS module is not actively cooled, i.e., no way to transfer heat other than by heat conduction. Here V_{QD} was varied between 10 and 60 mV. The temperature sensors on the *RE*BCO stacks #1, #7, #13, and #19 as well as the sensors located in the copper end cap at the warm end of the *RE*BCO module were analyzed together with the warm end stack voltages and the total voltage along the module. In particular, the correlation between the measured total voltage (used for quench detection) and the maximum temperature was investigated. Figure 12 shows the temperature $T_{HTS95\%}$ at the four stacks at 95% in length measured from the copper-stainless steel interface at the cold end as a function of time for 20 kA and different V_{QD}. The temperature evolution is identical for the different runs, i.e. the temperatures measured for $V_{QD} = 10$ mV are on top of those measured for $V_{QD} =$ 30 mV, 40 mV, 50 mV, and 60 mV, respectively. In particular, stack #7 has always a lower temperature than stacks #1, 13, and 19. The maximum temperatures for the different runs were fitted with a second order polynomial and it can be seen that this curve changes its slope which could be an

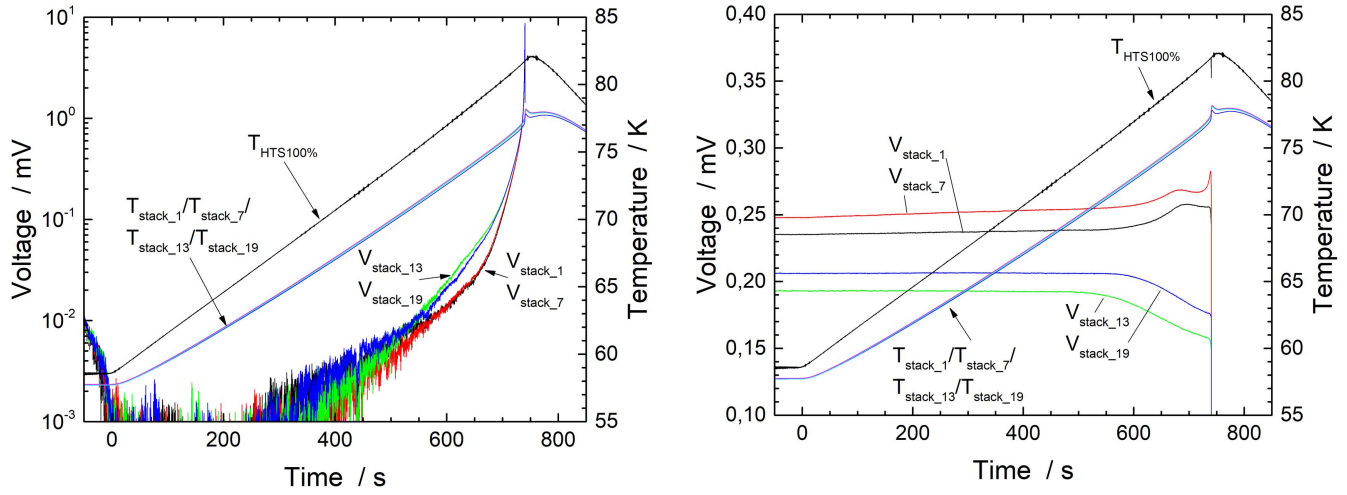

Figure 10. Voltage of the four stacks at the warm (left) and cold (right) end during LOFA at 20 kA.

Table 4. Main results of the pulse tests of the *RE*BCO and Bi-2223 current leads for 1 kA s^{-1} and 10 kA ramp rates.

HTS module	*RE*BCO	Bi-2223	*RE*BCO	Bi-2223
Ramp rate	1 kA s^{-1}		10 kA s^{-1}	
50 K He mass flow rate used in experiment	0.99 g s^{-1}		0.99 g s^{-1}	
Pulse repetition time	104 s		65 s	
$T_{HTS100\%}$ drop at beginning of pulsing	−1.29 K	−0.99 K	−0.72 K	−0.56 K
$T_{HTS100\%}$ increase during pulsing	0.24 K	0.25 K	1.47 K	1.63 K
Total $T_{HTS100\%}$ change	−1.05 K	−0.74 K	+0.75 K	+1.07 K
Average DC current in experiment	12.90 kA		13.855 kA	
Corresponding He mass flow rate	0.94 g s^{-1}		1.005 g s^{-1}	
Heat load increase at 4.5 K during pulsing	(2.068 ± 0.02) W	(1.330 ± 0.01) W	(2.614 ± 0.02) W	(1.794 ± 0.02) W
DC heat load $P_{DC} = R_C I_{equ}{}^2$	(2.087 ± 0.07) W	(1.443 ± 0.07) W	(2.407 ± 0.08) W	(1.664 ± 0.08) W
AC losses	(−0.019 ± 0.07) W	(−0.113 ± 0.07) W	(0.207 ± 0.08) W	(0.130 ± 0.08) W
Calculated AC losses incl. bus bar and joint box	0.0112 W	0.0108 W	0.174 W	0.168 W

Table 5. Summary of the main results of the LOFA tests.

Current	T_{CS}	T_Q	LOFA time	Time $T_Q - T_{CS}$	Time T_Q till current switch-off
			*RE*BCO current lead		
16 kA	(81.2 ± 0.3) K	(83.1 ± 0.1) K	1013 s	387 s	15.65 s
18 kA	(80.1 ± 0.3) K	(82.2 ± 0.1) K	809 s	272 s	12.31 s
20 kA	(79.2 ± 0.3) K	(81.3 ± 0.1) K	740 s	314 s	11.83 s
			Bi-2223 current lead		
20 kA	(84.6 ± 0.4) K	(91.0 ± 0.1) K	845 s	479 s	57.83 s

indicator for the fact that the location of the maximum temperature moves away.

Figure 13 shows the warm end stack voltage as a function of the temperature at 95% of the stack length $T_{HTS95\%}$ for $V_{QD} = 60$ mV. A very sharp voltage-temperature transition can be seen. Afterwards, i.e., for voltages between 30 mV and 50 mV, the temperature increase is about 1 K mV^{-1}.

Figure 14 shows the voltage along the *RE*BCO module during quench at 20 kA and comparison to that of the Bi-2223-module of the W7-X prototype CL at 18.2 kA. In the legend of the figure the current density in the stabilizer, i.e., brass for the *RE*BCO module and AgAu for the Bi-2223-module, is also given. The time difference between the voltage reaching 10 and 50 mV is only 2.5 s and much shorter than for the Bi-2223-module for which it is 6 s. Again, the different stabilizer resistances play a role. This has to be taken into account as the CL is operating together with a magnet.

The equivalent decay time constant of a magnet is calculated by equalizing the average energy for both current cases.

$$\frac{E}{R} = \int_0^\infty I(t)^2 \mathrm{d}t = I^2 \int \mathrm{e}^{-2t/\tau}\,\mathrm{d}t = \frac{2I^2}{\tau} = \frac{I^2}{T}. \qquad (7)$$

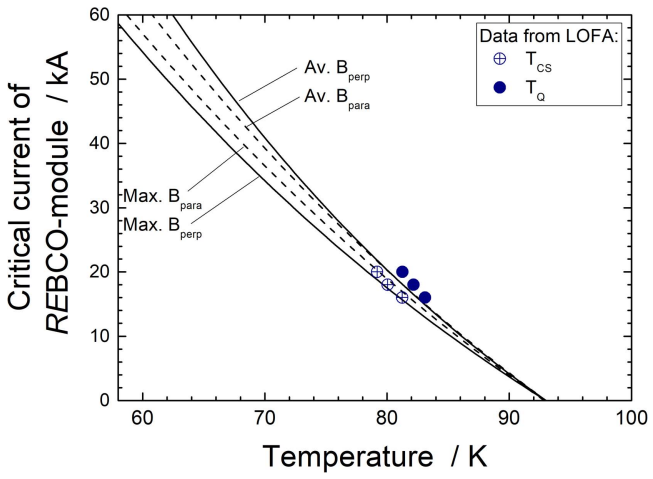

Figure 11. Critical current scaled from single tape at average and maximum magnetic field perpendicular and parallel to the *ab*-plane as a function of temperature and measured current sharing temperature T_{CS} and quench temperature T_Q.

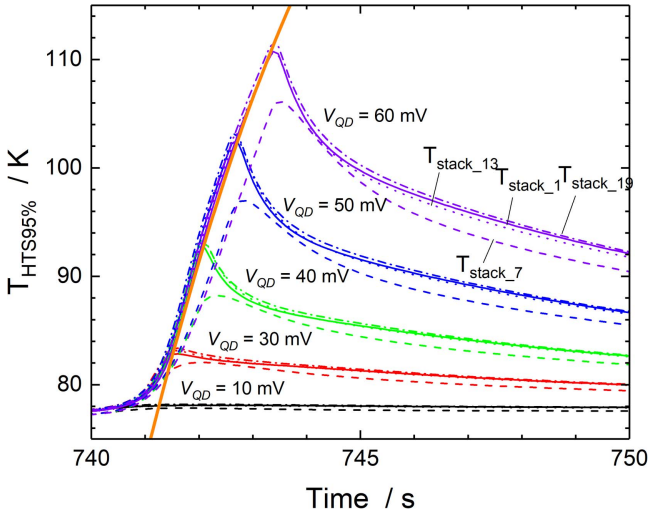

Figure 12. Temperatures $T_{HTS95\%}$ at the four stacks at 95% in length measured from the copper-stainless steel interface at the cold end as a function of time for 20 kA and different V_{QD}. The results of a second order polynomial fit are also shown as thick full line.

From this, $T = \tau/2$, i.e., the linear time duration is equal to half of the exponential decay time constant. In addition, the time delay from the QD system t_{del1} and the time delay due to the current switches t_{del2} have to be considered, too. This leads to the following correlation:

$$\tau = 2(T_{meas} - t_{del1} - t_{del2}). \quad (8)$$

If taking 10 mV as quench detection voltage and using $t_{del1} + t_{del2} = 0.6$ s, which is a reasonable time in a magnet system like e.g. in W7-X [19], one gets a discharge time constant of 3.8 s which is OK for W7-X (equivalent time constant of $\tau = 3.5$ s) but too small for other systems like in JT-60SA, ITER, or even in DEMO. A lower quench detection voltage will be necessary for such systems. It should be noted

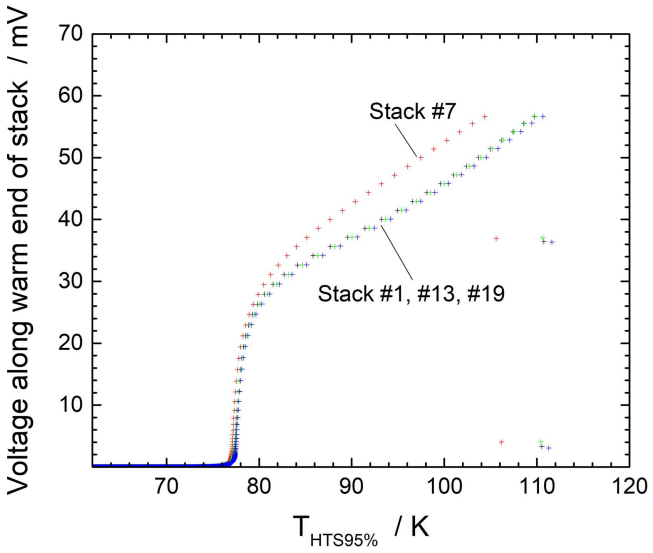

Figure 13. Warm end stack voltage as a function of the temperature at 95% of the stack length $T_{HTS95\%}$ for $V_{QD} = 60$ mV.

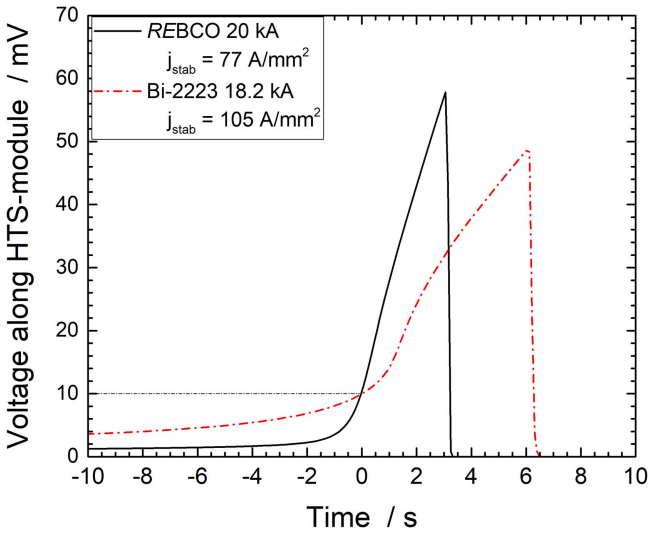

Figure 14. Voltage along the *RE*BCO module during quench at 20 kA (full line) as a function of time. The results of the Bi-2223-module measured during a quench of the W7-X prototype CL at 18.2 kA are shown for comparison (dashed–dotted line). Both voltages are time correlated at 10 mV.

that in the HTS CLs design for ITER, a quench detection threshold of 3 mV has been chosen [20].

4. Summary

KIT has developed a 20 kA HTS CL using *RE*BCO material. The *RE*BCO module is designed as close as possible to the design of the Bi-2223 module developed for the HTS CLs for JT-60SA to ease comparison. A three-fold stack design is chosen to place the required number of tapes on the outer surface of the structure. Staircase contacts at both ends were designed to guarantee current transfer from the copper end caps to the *RE*BCO tapes.

Table 6. Summary of the main results of the *RE*BCO CL tests and comparison to the JT-60SA CL tests.

Parameter	*RE*BCO CL	Bi-2223 CL (JT-60SA)
Maximum current	20 kA	20 kA
He mass flow rate at 20 kA	$(1.58 + 0.023 \pm 0.047)$ g s^{-1}	$(1.58 + 0.023 \pm 0.048)$ g s^{-1}
He mass flow rate at 0 kA	$(0.48 + 0.034 \pm 0.014)$ g s^{-1}	$(0.48 + 0.034 \pm 0.014)$ g s^{-1}
Heat load at 4.5 K end without current	(2.91 ± 1) W	(3.04 ± 1) W
Transition resistance at cold end of HTS part	(10.18 ± 0.43) nΩ	(6.13 ± 0.39) nΩ
Transition resistance at warm end of HTS part	(17.53 ± 0.44) nΩ	(12.76 ± 0.43) nΩ
LOFA time at 20 kA	12.3 min	14 min
Current sharing temperature	(79.2 ± 0.3) K	(84.6 ± 0.4) K

After assembly at KIT the *RE*BCO CL has been tested together with a JT-60SA CL in the test facility CuLTKa. The results for the *RE*BCO CL are summarized as follows.

- The heat load at 4.5 K without current is about 3 W.
- The helium mass flow rate at 0 kA is 0.48 g s^{-1} and at 20 kA 1.58 g s^{-1}.
- The contact resistances between the *RE*BCO module at the cold and warm end are larger than those of the Bi-2223 module but as expected from the three-fold stack mock-ups built during the R&D phase.
- The pulsed operation with trapezoidal pulses of 1 and 10 kA s^{-1} ramp rates and constant mass flow rate of 1 g s^{-1} show no strong temperature change during pulsing.
- The time during LOFA simulation is significantly shorter for the *RE*BCO CL than for the Bi-2223 one because of the much lower critical temperature but it is still more than 12 min.
- The temperature increase during quench is about 1 K mV^{-1} between 30 and 50 mV.
- The time between the voltage reaching 10 and 50 mV is only $T = 2.5$ s which has to be considered when operating the CL to feed a magnet.

Table 6 summarizes the main results of the *RE*BCO CL tests to compare them to those of the Bi-2223 CL tests. The slightly higher He mass flow rate for the Bi-2223 CL at 20 kA is certainly not caused by the use of the Bi-2223 module rather than the *RE*BCO module; the higher contact resistance at the HTS-HX interface for the *RE*BCO CL would lead to a slightly larger He mass flow rate than for the Bi-2223 CL. On the other hand, the connection to the infrastructure like the water-cooled cables influences the performance as well. More detailed simulations of the CL performance both in steady state and in pulse operation where the interfaces to the infrastructure are included are in [16].

As a conclusion, it can be said that in normal operating conditions the *RE*BCO CL behaves very similar to a Bi-2223 one. In case of abnormal conditions, e.g. during LOFA and quench, the *RE*BCO CL has a shorter LOFA time which is caused by the lower critical temperature and a significantly shorter quench evolution time which means that less time is available to switch-off the current.

Acknowledgments

The authors appreciate the effort of the main workshop of KIT and the current lead assembly crew as well as the refrigerator and testing group in the ITEP. This work is financially supported by the German Ministry of Research and Education BMBF under the grant No. 03FUS0019. The views and opinions expressed herein do not reflect necessarily those of the BMBF.

ORCID iDs

R Heller https://orcid.org/0000-0002-6600-1861

References

[1] Heller R, Fietz W H, Kienzler A and Lietzow R 2011 High temperature superconductor current leads for fusion machines *Fusion Eng. Des.* **86** 1422–6
[2] Heller R *et al* 2005 Experimental results of a 70 kA high temperature superconductor current lead demonstrator for the ITER magnet system *IEEE Trans. Appl. Supercond.* **15** 1496–9
[3] Wesche R, Heller R, Bruzzone P, Fietz W H, Lietzow R and Vostner A 2007 Design of high temperature superconductor current leads for ITER *Fusion Eng. Des.* **82** 1385–90
[4] Heller R *et al* 2011 Test results of the high temperature superconductor prototype current leads for Wendelstein 7-X *IEEE Trans. Appl. Supercond.* **21** 1062–5
[5] Tsunematsu T 2009 Broader approach to fusion energy *Fusion Eng. Des.* **84** 122–4
[6] Heller R, Fietz W H, Heiduk M, Hollik M, Kienzler A, Lange C, Lietzow R, Meyer I and Richter T 2018 Overview of JT-60SA HTS current lead manufacture and testing *IEEE Trans. Appl. Supercond.* **28** 4800105
[7] Wesche R, Bykovsky N, Uglietti D, Sedlak K, Stepanov B and Bruzzone P 2016 Commissioning of HTS adapter and heat exchanger for testing of high-current HTS conductors *IEEE Trans. Appl. Supercond.* **26** 9500705
[8] Saggese A, Iannone G, Gambardella U, Califano N and Ferrentino A 2015 20 kA HTS current leads for the INFN magnet test facility *IEEE Trans. Appl. Supercond.* **25** 4801304
[9] Kovalev I A, Surin M I, Naumov A V, Novikov M S, Novikov I, Ilin A A, Polyakov A V, Scherbakov V I and Shutova D I 2017 Test results of 12/18 kA ReBCO coated conductor current leads *Cryogenics* **85** 71–7

[10] Drotziger S, Fietz W H, Heller R and Jung A 2016 Investigation of stabilizer material properties used with *RE*BCO coated conductor tapes for the application in a 20 kA high-temperature superconductor current lead *IEEE Trans. Appl. Supercond.* **26** 4801409

[11] Heller R, Bagrets N, Fietz W H, Gröner F, Kienzler A, Lange C and Wolf M J 2017 Towards a 20 kA high temperature superconductor current lead module using *RE*BCO tapes *Supercond. Sci. Technol.* **31** 015021

[12] Zappatore A, Heller R, Savoldi L and Zanino R 2017 Assessment of the performance of a 20 kA REBCO current lead *CHATS on Applied Superconductivity 2017 Workshop (Sendai, Japan, 10–12 December)*

[13] Friesinger G and Heller R 1993 Use of Nb_3Sn inserts in a forced flow cooled 30 kA current lead *Appl. Supercond.* **2** 21–7

[14] Heller R, Fink S, Friesinger G, Kienzler A, Lingor A, Schleinkofer G, Süsser M, Ulbricht A, Wüchner F and Zahn G 2001 Development of forced flow cooled current leads for fusion magnets *Cryogenics* **41** 201–11

[15] Richter T, Bobien S, Fietz W H, Heiduk M, Heller R, Hollik M, Lange C, Lietzow R and Rohr P 2017 Design, construction and performance of the current lead test facility CuLTKa *Cryogenics* **86** 22–9

[16] Zappatore A, Heller R, Savoldi L and Zanino R 2017 Modelling of the test of the JT-60SA HTS current leads *Cryogenics* **85** 78–87

[17] Drotziger S, Fietz W H, Heiduk M, Heller R, Lange C, Lietzow R and Möhring T 2012 Investigation of HTS current leads under pulsed operation for JT-60SA *IEEE Trans. Appl. Supercond.* **22** 4801704

[18] Nakamura K, Nishimura K, Masuda T, Takao T, Murakami H and Yoshida K 2011 AC loss and temperature margin of cable-in-conduit conductors for JT-60SA poloidal field coil *IEEE Trans. Appl. Supercond.* **21** 2016–9

[19] Rummel T, Gaupp O, Lochner G and Sapper J 2002 Quench protection for the superconducting magnet system of WENDELSTEIN 7-X *IEEE Trans. Appl. Supercond.* **12** 1382–5

[20] Ding K *et al* 2012 Development of ITER HTS current lead at ASIPP *Phys. Proc.* **36** 931–6